$\gamma^*\gamma^* \to \eta_c(1S,2S)$ transition form factors for spacelike photons

Izabela Babiarz,[1,*] Victor P. Goncalves,[2,†] Roman Pasechnik,[3,‡] Wolfgang Schäfer,[1,§] and Antoni Szczurek[4,¶]

[1]*Institute of Nuclear Physics Polish Academy of Sciences,*
ul. Radzikowskiego 152, PL-31-342 Kraków, Poland
[2]*Instituto de Física e Matemática—Universidade Federal de Pelotas (UFPel)*
CP 354, CEP 96010-900, Pelotas—RS—Brazil
[3]*Department of Astronomy and Theoretical Physics, Lund University, SE-223 62 Lund, Sweden*
[4]*Faculty of Mathematics and Natural Sciences, University of Rzeszów,*
ul. Pigonia 1, PL-35-310 Rzeszów, Poland

We derive the light-front wave function (LFWF) representation of the $\gamma^*\gamma^* \to \eta_c(1S), \eta_c(2S)$ transition form factor $F(Q_1^2, Q_2^2)$ for two virtual photons in the initial state. For the LFWF, we use different models obtained from the solution of the Schrödinger equation for a variety of $c\bar{c}$ potentials. We compare our results to the *BABAR* experimental data for the $\eta_c(1S)$ transition form factor, for one real and one virtual photon. We observe that the onset of the asymptotic behavior is strongly delayed and discuss applicability of the collinear and/or massless limit. We present some examples of two-dimensional distributions for $F(Q_1^2, Q_2^2)$. A factorization breaking measure is proposed and factorization breaking effects are quantified and shown to be almost model independent. Factorization is shown to be strongly broken, and a scaling of the form factor as a function of $\bar{Q}^2 = (Q_1^2 + Q_2^2)/2$ is obtained.

I. INTRODUCTION

The description of the hadronic structure in terms of the quark and gluon degrees of freedom is one of the main goals of quantum chromodynamics (QCD). During the last years, our understanding about the partonic distributions has been substantially improved by the experimental data obtained in ep and pp colliders. Complementary information about the internal structure of mesons can be accessed by the study of the electromagnetic form factors and the meson-photon transition form factors. There has been a lot of interest recently in the exclusive production of mesons via photon fusion processes studied mainly at the e^+e^- colliders [1]. Such studies are strongly motivated by the expectation that at large photon virtualities the measurements of the cross sections will provide strong constraints in the probability amplitude for finding partons in the mesons [2–4]. The meson-photon transition form factors

are also of interest because of the role they play in the hadronic light-by-light contribution to the muon anomalous magnetic moment [5].

During the last years, a lot of attention has been paid to the case of pseudoscalar light meson-photon transition form factors [6,7], mainly motivated by the experimental data from the CLEO, *BABAR*, Belle, and L3 collaborations for the π^0, η, and η' production in e^+e^- collisions. These collaborations have extracted the transition form factor from single-tag events where only one of the leptons in the final state is measured. In this case, one of the photons is far off the mass shell, while the other is almost real. Such data have allowed testing of the collinear factorization approach and the onset of the asymptotic regime, as well as motivated the improvement of theoretical approaches. Similar results have been obtained for η_c production. In this case, the η_c mass provides a hard scale that justifies the use of a perturbative approach even for zero virtualities. In the past this transition form factor was studied in different approaches, (although often only for one virtual photon), such as perturbative QCD [8,9], lattice QCD [10,11], nonrelativistic QCD [12,13], QCD sum rules [14], as well as from Dyson-Schwinger and Bethe-Salpeter equations [15]. In the light-front quark model (LFQM) the case of one virtual and one real photon has been studied in [16,17].

In the present paper we will treat the heavy meson-photon transition form factor, focusing our analysis on the pseudoscalar charmonium state $\eta_c(1S)$ and its radial

*izabela.babiarz@ifj.edu.pl
†barros@ufpel.edu.br
‡roman.pasechnik@thep.lu.se
§Wolfgang.Schafer@ifj.edu.pl
¶antoni.szczurek@ifj.edu.pl

excitation $\eta_c(2S)$. Here we will focus on calculating the transition form factor for both virtual photons, which was not studied so far in the light-front approach. These double virtual transition form factors can be measured in e^+e^- collisions in the double-tag mode, where both the electron and the positron are detected in the final state. Recent results for the η' production by the *BABAR* Collaboration [18] have demonstrated that this study is feasible. Our study is motivated by the possibility of an accurate measurement of the double virtual transition form factors considering the high luminosity expected at Belle2. This may open new possibilities, such as the issue of factorization breaking of the transition form factors, which will be addressed in this paper. Regarding the wave functions of the quarkonia, we wish to use also $c\bar{c}$ wave functions obtained from realistic potential models. Here we will make use of the solutions obtained in [19]. We shall investigate how well they can describe the recent *BABAR* data [20] for $\gamma\gamma^* \rightarrow \eta_c(1S)$. We shall also calculate transition form factors for $\gamma\gamma^* \rightarrow \eta_c(2S)$, not yet measured, but could be considered for the Belle 2 program.

The paper is organized as follows. In Sec. II, we present the light-front formalism that is used for computations of the $\gamma^*\gamma^* \rightarrow \eta_c$ form factor. Here, we provide the details of the light front $\eta_c(1S, 2S)$ wave function calculations in the framework of the Schrödinger equation with a chosen set of $c\bar{c}$ interaction potentials, as well as derive the basic relations for the corresponding amplitude and the transition form factor. In Sec. III, we discuss the most relevant numerical results on the η_c wave functions and the transition form factors for different $c\bar{c}$ potentials, which are also compared to the existing *BABAR* data for the $\eta_c(1S)$ state. Section IV summarizes the most important results of our analysis.

II. THE LIGHT-FRONT FORMALISM FOR THE $\gamma^*\gamma^* \rightarrow \eta_c$ FORM FACTOR

Our goal in this section is to describe the $\gamma^*\gamma^* \rightarrow \eta_c$ form factor, which can be measured in e^+e^- collisions using two-photon events in which both photons are far off the mass shell. The typical diagram is represented in Fig. 1. We will consider the light-front formalism, which allows us to describe the meson in terms of the quark degrees of freedom. Let us first start from general kinematical considerations.

The amplitude for the photon fusion $\gamma^*\gamma^* \rightarrow \eta_c$ has the general form dictated by the $J^{PC} = 0^{-+}$ quantum numbers of the η_c:

$$\mathcal{M}_{\mu\nu}(\gamma^*(q_1)\gamma^*(q_2) \rightarrow \eta_c)$$
$$= 4\pi\alpha_{\text{em}}(-i)\varepsilon_{\mu\nu\alpha\beta}q_1^{\alpha}q_2^{\beta}F(Q_1^2, Q_2^2). \quad (2.1)$$

Here $Q_i^2 = -q_i^2 \geq 0$, $i = 1, 2$ are the virtualities of photons, which we take both to be spacelike. The form factor
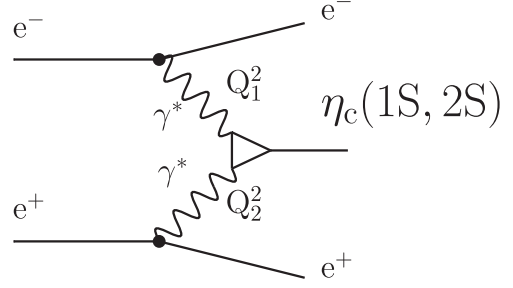

FIG. 1. The η_c production by the interaction of two virtual photons in e^+e^- collisions.

$F(Q_1^2, Q_2^2)$ above is the object of interest in this paper. It is normalized such that the two-photon decay-width of the meson is obtained from

$$\Gamma(\eta_c \rightarrow \gamma\gamma) = \frac{\pi}{4}\alpha_{\text{em}}^2 M_{\eta_c}^3 |F(0, 0)|^2. \quad (2.2)$$

For further calculation it is useful to choose a frame in which incoming photon four-momenta have the form

$$q_1 = q_1^+ n^+ + q_{1\perp}, \qquad q_2 = q_2^- n^- + q_{2\perp}. \quad (2.3)$$

Here

$$n^{\pm} = \frac{1}{\sqrt{2}}(1, 0, 0, \pm 1), \quad (2.4)$$

and we will denote the transverse vectors by boldface vectors, e.g.,

$$q_{i\perp} = (0, \boldsymbol{q}_i, 0), \qquad q_{i\perp}^2 = -\boldsymbol{q}_i^2. \quad (2.5)$$

As the polarization vectors of off-shell photons we will choose n^+ and n^- for the first and second photon, respectively. The four-momenta of photons satisfy $n^+ \cdot q_1 = n^- \cdot q_2 = 0$.[1] We finally note that the transverse momentum of the meson is $\boldsymbol{P} = \boldsymbol{q}_1 + \boldsymbol{q}_2$, and the photon light-front momenta fulfill

$$2q_1^+ q_2^- = M_{\eta_c}^2 + \boldsymbol{P}^2. \quad (2.6)$$

Projected onto the photon polarizations, the amplitude takes the simple form

$$n^{+\mu}n^{-\nu}\mathcal{M}_{\mu\nu}(\gamma^*(q_1)\gamma^*(q_2) \rightarrow \eta_c)$$
$$= 4\pi\alpha_{\text{em}}(-i)[\boldsymbol{q}_1, \boldsymbol{q}_2]F(Q_1^2, Q_2^2), \quad (2.7)$$

where $[\boldsymbol{q}_1, \boldsymbol{q}_2] = q_1^x q_2^y - q_1^y q_2^x$.

---

[1]Notice, that these polarizations are precisely the polarizations which dominate at high energies; see the diagram represented in Fig. 1. (See e.g., chapter 8 of [21].)

A. Light-front wave function of η_c

We treat the η_c as a bound state of a charm quark and antiquark, thus assuming that the dominant contribution comes from the $c\bar{c}$ component in the Fock-state expansion:

$$|\eta_c; P_+, \boldsymbol{P}\rangle = \sum_{i,j,\lambda,\bar{\lambda}} \frac{\delta_j^i}{\sqrt{N_c}} \int \frac{dz d^2\boldsymbol{k}}{z(1-z)16\pi^3} \Psi_{\lambda\bar{\lambda}}(z, \boldsymbol{k})$$
$$\times |c_{i\lambda}(zP_+, \boldsymbol{p}_c)\bar{c}_{\bar{\lambda}}^j((1-z)P_+, \boldsymbol{p}_{\bar{c}})\rangle + \dots$$
$$(2.8)$$

Here the c-quark and $\bar{c}$-antiquark carry a fraction z and $1-z$ respectively of the η_c's plus-momentum. The light-front helicites of quark and antiquark are denoted by λ, $\bar{\lambda}$, and take values ± 1. The transverse momenta of quark and antiquark are

$$\boldsymbol{p}_c = \boldsymbol{k} + z\boldsymbol{P}, \qquad \boldsymbol{p}_{\bar{c}} = -\boldsymbol{k} + (1-z)\boldsymbol{P}. \quad (2.9)$$

The contribution of higher Fock states is expected to be suppressed at large Q^2. Moreover, the fact that nonrelativistic potential models are able to describe the quarkonia properties implies that the valence $c\bar{c}$ Fock state probability of η_c is almost 1 (see e.g., [8,22]). In Ref. [16], the authors have assumed the η_c wave function is a combination of the $u\bar{u}$, $d\bar{d}$, $s\bar{s}$, and $c\bar{c}$ Fock states. The resulting predictions for the η_c form factor become dependent on the assumptions for the mixing angles, but are similar to those obtained assuming that the η_c is a pure $c\bar{c}$ state. Therefore, our assumption for the η_c wave function as a pure $c\bar{c}$ state is a very good approximation. The light-front wave function encodes all the necessary information on the bound state. Recently there has been a lot of interest in calculating light-front wave functions of heavy quarkonia; see for example [23–25]. Here we follow a different approach which relies on a prescription due to Terentev [26], valid for weakly bound nonrelativistic systems, which expresses the light-front wave function in terms of the rest-frame Schrödinger wave function.

In the $^{2S+1}L_J = {}^1S_0$ state the wave function of the two-body system for canonical spin-projections $\sigma\bar{\sigma}$ of quark and antiquark has the form

$$\Psi_{\sigma\bar{\sigma}}(\vec{p}) = \frac{1}{\sqrt{2}} \chi_\sigma^\dagger i\sigma_2 \chi_{\bar{\sigma}} \phi(p) Y_{00}\left(\frac{\vec{p}}{p}\right)$$
$$= \frac{1}{\sqrt{2}} \chi_\sigma^\dagger i\sigma_2 \chi_{\bar{\sigma}} \frac{u(p)}{p} \frac{1}{\sqrt{4\pi}}. \quad (2.10)$$

Here $\chi^\dagger$, χ are the Pauli spinors, and $p = |\vec{p}|$. The normalization condition reads

$$\int d^3\vec{p} \sum_{\sigma\bar{\sigma}} |\Psi_{\sigma\bar{\sigma}}(\vec{p})|^2 = 1, \quad \int_0^\infty dp u^2(p) = 1. \quad (2.11)$$

In order to apply Terentev's transformation, we first introduce the relative momentum $\vec{p}$ of quark and antiquark in the center-of-mass frame at fixed invariant mass $M_{c\bar{c}}$,

$$\boldsymbol{p} = \boldsymbol{k}, \quad p_z = \left(z - \frac{1}{2}\right)M_{c\bar{c}}, \quad (2.12)$$

so that

$$\vec{p}^2 = \frac{1}{4}(M_{c\bar{c}}^2 - 4m_c^2) = \frac{1}{4}\left(\frac{\boldsymbol{k}^2 + m_c^2}{z(1-z)} - 4m_c^2\right). \quad (2.13)$$

We then decompose the helicity dependent light-front wave function into a spin/momentum and radial part as

$$\Psi_{\lambda\bar{\lambda}}(z, \boldsymbol{k}) = \frac{\Gamma_{\lambda\bar{\lambda}}(z, \boldsymbol{k})}{\mathcal{N}(z, \boldsymbol{k})} \phi(z, \boldsymbol{k}). \quad (2.14)$$

To obtain the helicity dependent part of the LFWF one needs to transform the rest-frame spinors to the light-front spinors, which is effected by means of a Melosh transform [27]. This has been done e.g., in Ref. [28], and the helicity-dependent vertex reads

$$\Gamma_{\lambda\bar{\lambda}}(z, \boldsymbol{k}) = \bar{u}_\lambda(zP_+, \boldsymbol{k})\gamma_5 v_{\bar{\lambda}}((1-z)P_+, -\boldsymbol{k})$$
$$= \frac{1}{\sqrt{z(1-z)}}\{\lambda m_c \delta_{\lambda-\bar{\lambda}} - \lambda\sqrt{2}\boldsymbol{k} \cdot e(-\lambda)\delta_{\lambda\bar{\lambda}}\},$$
$$(2.15)$$

where $e(\lambda) = -(\lambda e_x + ie_y)/\sqrt{2}$. The normalizing function $\mathcal{N}$ is

$$\mathcal{N}(z, \boldsymbol{k}) = \left(\sum_{\lambda\bar{\lambda}} \Gamma_{\lambda\bar{\lambda}}(z, \boldsymbol{k})\Gamma_{\lambda\bar{\lambda}}^*(z, \boldsymbol{k})\right)^{1/2}$$
$$= \sqrt{2}\sqrt{\frac{\boldsymbol{k}^2 + m_c^2}{z(1-z)}} = \sqrt{2}M_{c\bar{c}}. \quad (2.16)$$

Then, if we take the meson state to obey the canonical relativistic normalization

$$\langle\eta_c; P'_+, \boldsymbol{P}'|\eta_c; P_+, \boldsymbol{P}\rangle = 2P_+(2\pi)^3\delta(P'_+ - P_+)\delta^{(2)}(\boldsymbol{P}' - \boldsymbol{P}),$$
$$(2.17)$$

the radial light-front wave function $\phi(z, \boldsymbol{k})$ will be normalized as

$$\int_0^1 \frac{dz}{z(1-z)} \int \frac{d^2\boldsymbol{k}}{16\pi^3} |\phi(z, \boldsymbol{k})|^2 = N_{c\bar{c}} = 1. \quad (2.18)$$

To relate the radial LFWF to the rest-frame wave function, we should still take into account a jacobian from changing the integration measure

$$\frac{dz d^2 \boldsymbol{k}}{z(1-z)} = 4 \frac{d^3 \vec{p}}{M_{c\bar{c}}}, \qquad (2.19)$$

so that we obtain the identification

$$\phi(z, \boldsymbol{k}) = \pi \sqrt{M_{c\bar{c}}} \frac{u(p)}{p}. \qquad (2.20)$$

To lighten up the notation of the amplitude, we also use

$$\psi(z, \boldsymbol{k}) = \frac{\phi(z, \boldsymbol{k})}{\mathcal{N}(z, \boldsymbol{k})} = \frac{\pi}{\sqrt{2M_{c\bar{c}}}} \frac{u(p)}{p}, \qquad (2.21)$$

which we also refer to as the radial wave function.

Let us now present the details of computation of the radial wave function by means of the Schödinger equation with a set of chosen $c\bar{c}$ interaction potentials. For reviews on these topics, see e.g., Refs. [29,30].

B. Schrödinger equation and $c\bar{c}$ interaction potentials

The charmonium wave function is found in the quark-antiquark rest frame by solving the Schrödinger equation which for the radial wave function $\psi(r)$ can be written as (for more details see the appendix in Ref. [19])

$$\frac{\partial^2 u(r)}{\partial r^2} = (V_{\text{eff}}(r) - \epsilon) u(r),$$

$$u(r) = \sqrt{4\pi} r \psi(r),$$

$$\int_0^\infty |u(r)|^2 dr = 1, \qquad (2.22)$$

where

$$V_{\text{eff}}(r) = m_c V(r) + \frac{l(l+1)}{r^2}, \qquad \epsilon = m_c E, \qquad (2.23)$$

in terms of the interaction $c\bar{c}$ potential, $V(r)$. Here, we briefly describe several models for $V(r)$ chosen for our analysis.

(1) Harmonic oscillator:

$$V(r) = \frac{1}{2} m_c \omega^2 r^2, \qquad (2.24)$$

where for charmonia we adopt

$$\omega = \frac{1}{2}(M_{2S} - M_{1S}) \simeq 0.3 \text{ GeV},$$

$$m_c = 1.4 \text{ GeV}. \qquad (2.25)$$

For such a simple choice of the interaction potential one finds an analytic solution of the Schrödinger equation (2.22)

$$u(r) = \exp\left[-\frac{1}{4} m_c \omega r^2\right], \qquad (2.26)$$

yielding a Gaussian shape of the wave function.

(2) Cornell potential [31,32]:

$$V(r) = -\frac{k}{r} + \frac{r}{a^2}, \qquad k = 0.52, \qquad a = 2.34 \text{ GeV}^{-1}, \qquad (2.27)$$

and the charm quark mass is fixed to $m_c = 1.84$ GeV.

(3) Logarithmic potential [33]:

$$V(r) = -0.6635 \text{ GeV} + (0.733 \text{ GeV}) \log(r \cdot 1 \text{ GeV}), \qquad (2.28)$$

with $m_c = 1.5$ GeV.

(4) Effective power-law potential [34,35]:

$$V(r) = -6.41 \text{ GeV} + (6.08 \text{ GeV})(r \cdot 1 \text{ GeV})^{0.106}, \qquad (2.29)$$

assumes $m_c = 1.334$ GeV [36].

(5) Buchmüller-Tye (BT) potential [37]:

$$V(r) = \begin{cases} \frac{k}{r} - \frac{8\pi}{27} \frac{v(\lambda r)}{r}, & r \geq 0.01 \text{ fm} \\ -\frac{16\pi}{25} \frac{1}{r \ln w(r)} \left(1 + 2(\gamma_E + \frac{53}{75}) \frac{1}{\ln w(r)} - \frac{462}{625} \frac{\ln \ln w(r)}{\ln w(r)}\right), & r < 0.01 \text{ fm}, \end{cases} \qquad (2.30)$$

where $\gamma_E = 0.5772$ is the Euler constant, and the function $v(x)$ is known numerically from Ref. [37], and

$$w(r) = \frac{1}{\lambda_{\text{MS}}^2 r^2}, \qquad \lambda_{\text{MS}} = 0.509 \text{ GeV}, \qquad k = 0.153 \text{ GeV}^2, \qquad \lambda = 0.406 \text{ GeV}. \qquad (2.31)$$

Here, the charm quark mass is taken to be $m_c = 1.48$ GeV. One notices that the BT potential at small r has a Coulomb-like behavior, while at large r it has a stringlike behavior such that its difference from the Cornell potential is mainly at small r.

C. Light-front representation of the amplitude and transition form factor

Our calculation follows the standard procedure of perturbative QCD for exclusive processes. We regard the $\gamma^*\gamma^* \to c\bar{c}$ transition as a hard, perturbatively calculable process and convolute the amplitude with the bound state wave function. We will assume later that the charm quark mass m_c by itself is large enough to justify perturbation theory and apply our results even in the limit of vanishing photon virtualities. Following [38] [see Eq. (A7) therein], the photon fusion amplitude can be expressed as

$$\mathcal{M}_{\mu\nu}(\gamma^*(q_1)\gamma^*(q_2) \to \eta_c) = \frac{\text{Tr}\mathbb{1}_{\text{color}}}{\sqrt{N_c}} \int \frac{dz d^2\mathbf{k}}{z(1-z)16\pi^3} \sum_{\lambda\bar{\lambda}} \Psi^*_{\lambda\bar{\lambda}}(z,\mathbf{k}) \mathcal{M}_{\mu\nu}(\gamma^*(q_1)\gamma^*(q_2) \to c_\lambda(z,\mathbf{p}_c)\bar{c}_{\bar{\lambda}}(1-z,\mathbf{p}_{\bar{c}})). \quad (2.32)$$

Here

$$\mathcal{M}_{\mu\nu}(\gamma^*(q_1)\gamma^*(q_2) \to c_\lambda(z,\mathbf{p}_c)\bar{c}_{\bar{\lambda}}(1-z,\mathbf{p}_{\bar{c}}))$$
$$= 4\pi\alpha_{\text{em}}\bar{u}_\lambda(zP_+,\mathbf{p}_c)\left(\gamma_\mu \frac{\hat{p}_c - \hat{q}_1 + m_c}{t - m_c^2}\gamma_\nu + \gamma_\nu \frac{\hat{p}_c - \hat{q}_2 + m_c}{u - m_c^2}\gamma_\mu\right)v_{\bar{\lambda}}((1-z)P_+,\mathbf{p}_{\bar{c}}), \quad (2.33)$$

where $\hat{p} \equiv p^\mu\gamma_\mu$ is the standard Feynman amplitude including the t-channel and u-channel exchange of a quark. We can express the denominators of the propagators though LF variables:

$$u - m_c^2 = -\frac{1}{1-z}[\mathbf{l}_A^2 + \mu^2],$$
$$t - m_c^2 = -\frac{1}{z}[\mathbf{l}_B^2 + \mu^2]. \quad (2.34)$$

Here we introduce the notation

$$\mathbf{l}_A = \mathbf{p}_{\bar{c}} - (1-z)\mathbf{q}_1 = -\mathbf{k} + (1-z)\mathbf{q}_2,$$
$$\mathbf{l}_B = \mathbf{p}_c - z\mathbf{q}_1 = \mathbf{k} + z\mathbf{q}_2, \quad (2.35)$$

and

$$\mu^2 = z(1-z)\mathbf{q}_1^2 + m_c^2. \quad (2.36)$$

Contracting the Feynman amplitude with $n_\mu^+ n_\nu^-$ allows us to reduce the amplitude to a form where only simple spinor products of the form $\bar{u}\hat{n}^+v$, $\bar{u}\hat{n}^-u$, $\bar{v}\hat{n}^-v$ need to be performed. Using the spinors from Ref. [38], we obtain then[2]

$$n^{+\mu}n^{-\nu}\mathcal{M}_{\mu\nu}(\gamma^*(q_1)\gamma^*(q_2) \to \eta_c)$$
$$= 4\pi\alpha_{\text{em}}\frac{\text{Tr}\mathbb{1}_{\text{color}}}{\sqrt{N_c}}(-2)\int \frac{dz d^2\mathbf{k}}{\sqrt{z(1-z)}16\pi^3}\left\{\left[\frac{1}{\mathbf{l}_A^2 + \mu^2} - \frac{1}{\mathbf{l}_B^2 + \mu^2}\right]\left[i[\mathbf{k},\mathbf{q}_1](\Psi^*_{+-}(z,\mathbf{k}) - \Psi^*_{-+}(z,\mathbf{k}))\right.\right.$$
$$\left.\left. - \sqrt{2}m\left((e(-)\mathbf{q}_1)\Psi^*_{++}(z,\mathbf{k}) + (e(+)\mathbf{q}_1)\Psi^*_{--}(z,\mathbf{k})\right)\right] + \left[\frac{1-z}{\mathbf{l}_A^2 + \mu^2} + \frac{z}{\mathbf{l}_B^2 + \mu^2}\right]i[\mathbf{q}_1,\mathbf{q}_2](\Psi^*_{+-}(z,\mathbf{k}) - \Psi^*_{-+}(z,\mathbf{k}))\right\}. \quad (2.37)$$

Here, subscripts $\pm$ of the wave functions stand for helicities $\pm\frac{1}{2}$ of (anti)quarks. Inserting the explicit expressions for the helicity dependent wave functions given in Eq. (2.15), we observe that there is a large cancellation between the parallel and antiparallel helicity configurations, and only the last term $\propto [\mathbf{q}_1,\mathbf{q}_2]$ survives. It is then straightforward to read off our result for the $\gamma^*\gamma^* \to \eta_c$ form factor by comparing to Eq. (2.7):

$$F(Q_1^2, Q_2^2) = e_c^2\sqrt{N_c}4m_c \cdot \int \frac{dz d^2\mathbf{k}}{z(1-z)16\pi^3}\psi(z,\mathbf{k})\left\{\frac{1-z}{(\mathbf{k}-(1-z)\mathbf{q}_2)^2 + z(1-z)\mathbf{q}_1^2 + m_c^2} + \frac{z}{(\mathbf{k}+z\mathbf{q}_2)^2 + z(1-z)\mathbf{q}_1^2 + m_c^2}\right\}. \quad (2.38)$$

---

[2]We have dropped the terms $\propto \Psi^*_{+-} + \Psi^*_{-+}$, which vanish for the pseudoscalar state; see Eq. (2.15).

and then to perform the integration over the azimuthal angle of $\boldsymbol{k}$. Using

$$\int_0^{2\pi} \frac{d\phi}{2\pi} \frac{1}{A + B\cos\phi} = \frac{1}{\sqrt{A^2 - B^2}}, \tag{2.39}$$

we can obtain

$$F(Q_1^2, Q_2^2) = e_c^2 \sqrt{N_c} 4m_c \cdot \int \frac{dzkdk}{z(1-z)8\pi^2} \psi(z, \boldsymbol{k}) \left\{ \frac{1-z}{\sqrt{(\boldsymbol{k}^2 - m_c^2 - z(1-z)\boldsymbol{q}_1^2 - (1-z)^2\boldsymbol{q}_2^2)^2 + 4\boldsymbol{k}^2(m_c^2 + z(1-z)\boldsymbol{q}_1^2)}} \right.$$

$$\left. + \frac{z}{\sqrt{(\boldsymbol{k}^2 - m_c^2 - z(1-z)\boldsymbol{q}_1^2 - z^2\boldsymbol{q}_2^2)^2 + 4\boldsymbol{k}^2(m_c^2 + z(1-z)\boldsymbol{q}_1^2)}} \right\}. \tag{2.40}$$

This form puts into evidence, that the invariant form factor $F(Q_1^2, Q_2^2)$ is a function of $Q_1^2 = \boldsymbol{q}_1^2$ and $Q_2^2 = \boldsymbol{q}_2^2$ only. Notice that by Bose symmetry, the form factor must be a symmetric function of Q_1^2, Q_2^2. This is evidently not obvious from the representations Eq. (2.38) or Eq. (2.40), as the integrand is manifestly asymmetric in $\boldsymbol{q}_1$, $\boldsymbol{q}_2$. However, as will be demonstrated below by the numerical results, our representation has the required symmetry. In particular, in the limit of one on-shell photon, one must have that $F(Q^2) \equiv F(Q^2, 0) = F(0, Q^2)$, and the two different integral representations for $F(Q^2)$ which follow from Eq. (2.38) coincide with the ones found in Ref. [17], where their equivalence was also demonstrated numerically.

A number of limits of Eq. (2.38) are interesting. First, the value $F(0, 0)$ for two on-shell photons is related to the two-photon decay width by Eq. (2.2). Note that

$$F(0,0) = e_c^2 \sqrt{N_c} 4m_c \cdot \int \frac{dzd^2\boldsymbol{k}}{z(1-z)16\pi^3} \frac{\psi(z, \boldsymbol{k})}{\boldsymbol{k}^2 + m_c^2}. \tag{2.41}$$

Let us write this result as an integral over the three-momentum $\vec{p}$ and the radial wave function $u(p)$:

$$F(0,0)$$

$$= e_c^2 \sqrt{N_c} 4m_c \int \frac{4d^3\vec{p}}{M_{c\bar{c}} 16\pi^3} \frac{\psi(z, \boldsymbol{k})}{\boldsymbol{k}^2 + m_c^2}$$

$$= e_c^2 \sqrt{2N_c} \frac{m_c}{\pi} \int_0^\infty \frac{dppu(p)}{\sqrt{M_{c\bar{c}}^3(p^2 + m_c^2)}} \int_{-1}^1 \frac{d\cos\theta}{1 - \beta^2\cos^2\theta}$$

$$= e_c^2 \sqrt{2N_c} \frac{2m_c}{\pi} \int_0^\infty \frac{dppu(p)}{\sqrt{M_{c\bar{c}}^3(p^2 + m_c^2)}} \frac{1}{2\beta} \log\left(\frac{1+\beta}{1-\beta}\right). \tag{2.42}$$

Here we used that in polar coordinates $\boldsymbol{k}^2 = p^2\sin^2\theta$, hence $\boldsymbol{k}^2 + m_c^2 = (p^2 + m_c^2)(1 - \beta^2\cos^2\theta)$, where we introduced

$$\beta = \frac{p}{\sqrt{p^2 + m_c^2}}, \tag{2.43}$$

the velocity v/c of the quark in the $c\bar{c}$ center of mass frame. Similar results for the relativistic corrections to the decay width exist in the literature; see e.g., Ref. [39] and references therein. Notice that in these approaches typically the running of the mass $M_{c\bar{c}}$ with p is neglected.

In the nonrelativistic (NR) limit, where $p^2/m_c^2 \ll 1$, $\beta \ll 1$, the invariant mass $M_{c\bar{c}}$ approaches $M_{c\bar{c}} = 2m_c$. If we neglect the binding energy, and identify $2m_c = M_{\eta_c}$, we obtain

$$F(0, 0) = e_c^2 \sqrt{N_c} \sqrt{2} \frac{4}{\pi \sqrt{M_{\eta_c}^5}} \int_0^\infty dppu(p)$$

$$= e_c^2 \sqrt{N_c} \frac{4R(0)}{\sqrt{\pi M_{\eta_c}^5}}. \tag{2.44}$$

Here $R(0)$ is the value of the radial wave function $R(r) = u(r)/r$ at the origin. This yields the well-known result for the $\gamma\gamma$ width (see e.g., Table 2.2 in Ref. [40])

$$\Gamma(\eta_c \to \gamma\gamma) = \frac{4\alpha_{em}^2 e_c^4 N_c}{M_{\eta_c}^2} |R(0)|^2, \tag{2.45}$$

which serves as a check on our normalization. In the same limit, which amounts to an expansion around $\boldsymbol{k} = 0$ and $z = 1/2$ in Eq. (2.38), we can derive the transition form factor in the NRQCD-limit,

$$F(Q_1^2, Q_2^2) = e_c^2 \sqrt{N_c} \frac{4}{\sqrt{\pi M_{\eta_c}}} \frac{1}{Q_1^2 + Q_2^2 + M_{\eta_c}^2} R(0). \tag{2.46}$$

Still another interesting limit exists; namely at very large Q_i^2, the $\boldsymbol{k}$-smearing becomes unimportant, and one can neglect $\boldsymbol{k}$ in the hard matrix element of Eq. (2.38). Then only the LFWF appears under the $\boldsymbol{k}$ integral, and the hard scattering factorization in terms of the distribution amplitude emerges. We introduce the distribution amplitude (DA) at a scale μ_0^2 as

$$f_{\eta_c}\varphi(z,\mu_0^2) = \frac{1}{z(1-z)}\frac{\sqrt{N_c}4m_c}{16\pi^3}\int d^2\mathbf{k}\,\theta(\mu_0^2 - \mathbf{k}^2)\psi(z,\mathbf{k}).$$

$$(2.47)$$

The DA is conveniently normalized as

$$\int_0^1 dz\,\varphi(z,\mu_0^2) = 1, \qquad (2.48)$$

so that we can extract the so-called decay constant f_{η_c} from the integral over z in Eq. (2.47). The transition form factor simplifies to

$$F(Q_1^2,Q_2^2) = e_c^2 f_{\eta_c}\cdot\int_0^1 dz\left\{\frac{(1-z)\varphi(z,\mu_0^2)}{(1-z)^2Q_1^2 + z(1-z)Q_2^2 + m_c^2}\right.$$
$$\left.+\frac{z\varphi(z,\mu_0^2)}{z^2Q_1^2 + z(1-z)Q_2^2 + m_c^2}\right\}. \qquad (2.49)$$

This representation is valid in the limit of large photon virtualities Q_1^2, Q_2^2.

III. NUMERICAL RESULTS

In this section we will present our results for the doubly virtual transition form factor, which will be calculated for the different models for the meson wave function. A comparison with the current experimental data will be presented and the onset of the asymptotic regime will be discussed. Moreover, in order to estimate the factorization breaking in the transition form factor we will also estimate the normalized form factor, defined by

$$\tilde{F}(Q_1^2,Q_2^2) = \frac{F(Q_1^2,Q_2^2)}{F(0,0)}, \qquad (3.1)$$

which nicely quantifies the deviation from pointlike coupling. A popular model for the transition form factor is based on the vector dominance model (VDM) (see e.g., Ref. [20]), and reads

$$\tilde{F}(Q_1^2,Q_2^2) = \frac{M_{J/\Psi}^2}{Q_1^2 + M_{J/\Psi}^2}\cdot\frac{M_{J/\Psi}^2}{Q_2^2 + M_{J/\Psi}^2}. \qquad (3.2)$$

It features a factorized dependence on the photon virtualities, which we expect to be broken. In our analysis, we will quantify the factorization breaking of the transition form factor by estimating the quantity defined by

$$R(Q_1^2,Q_2^2) = \frac{\tilde{F}(Q_1^2,Q_2^2)}{\tilde{F}(Q_1^2,0)\tilde{F}(0,Q_2^2)}. \qquad (3.3)$$

A. $c\bar{c}$ wave functions of $\eta_c(1S)$ and $\eta_c(2S)$

Our wave functions $u(p)$ were obtained by Fourier transform from the r-dependent $c\bar{c}$ wave functions obtained as a solution of the Schrödinger equation with different, realistic potentials from the literature as described in the previous section. In Fig. 2 we show the wave function $u(p)$ for different potentials for the $1S$ state (upper panel) and for the $2S$ radial excitation (lower panel). We have that the different models predict similar shapes for the wave functions, but they differ in their predictions for the position of the peaks and the approach to the large momentum limit.

Using the Terentev prescription [see Eq. (2.12)] we obtain wave functions in the light-front variables z and $k_T = |\mathbf{k}|$. In Fig. 3 we show as an example the light-front wave function of Eq. (2.21) in the (z, k_T) space for the Buchmüller-Tye potential. As expected, the wave function is strongly peaked at $z \approx 1/2$ and is strongly suppressed in the endpoints. These properties
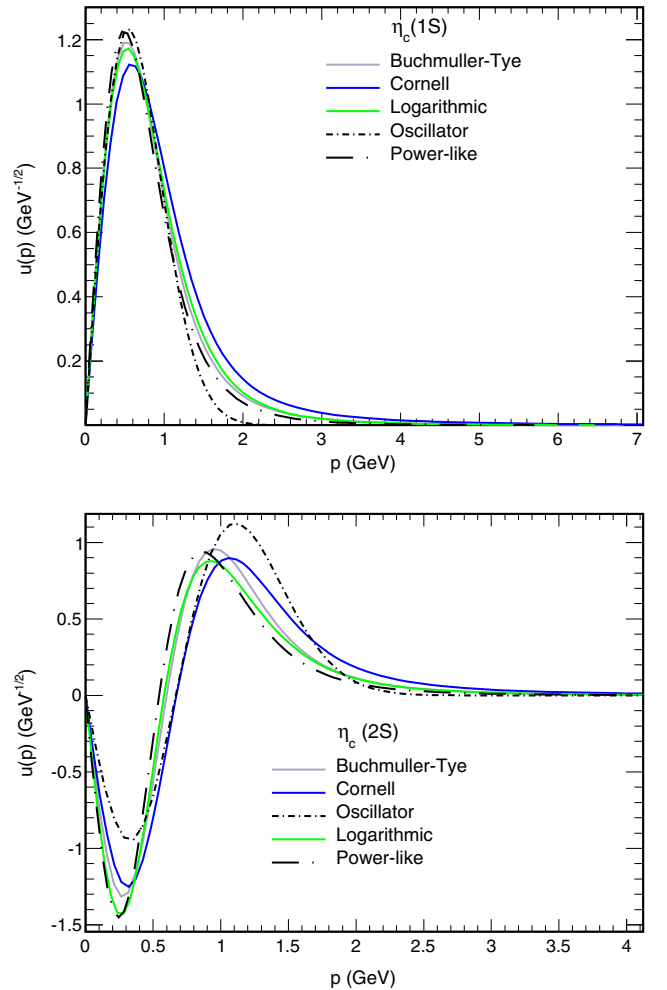

FIG. 2. Momentum space wave function $u(p)$ for $\eta_c(1S)$ (top) and $\eta_c(2S)$ (bottom) for different potentials.
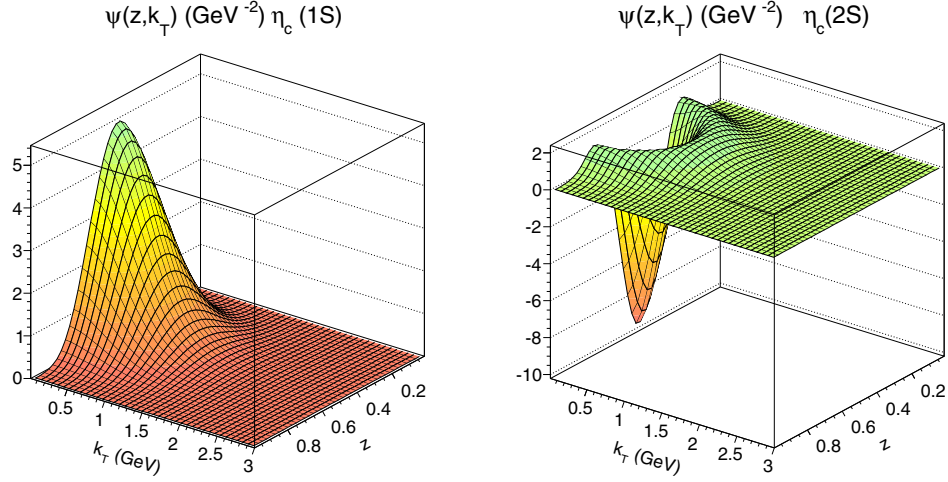
FIG. 3. The light-front radial wave function $\psi(z, \boldsymbol{k})$ of Eq. (2.21) in the (z, k_T) space for Buchmüller-Tye potential for $\eta_c(1S)$ and $\eta_c(2S)$, respectively. Here $k_T = |\boldsymbol{k}|$.

are shared by all wave functions for the potentials used by us. The Cornell potential wave function somewhat stands out as it has the hardest tail at large momenta.

B. $\gamma^* \gamma^*$ transition form factor

We start the presentation of our results from the value of $F(0,0)$ for $\eta_c(1S)$ and $\eta_c(2S)$ obtained from the different potential model wave functions. The obtained results for

TABLE I. Transition form factor $|F(0,0)|$ for $\eta_c(1S)$ at $Q_1^2 = Q_2^2 = 0$.

Potential type	m_c [GeV]	$|F(0,0)|$ [GeV^{-1}]	$\Gamma_{\gamma\gamma}$ [keV]	f_{η_c} [GeV]
Harmonic oscillator	1.4	0.051	2.89	0.2757
Logarithmic	1.5	0.052	2.95	0.3373
Powerlike	1.334	0.059	3.87	0.3074
Cornell	1.84	0.039	1.69	0.3726
Buchmüller-Tye	1.48	0.052	2.95	0.3276
Experiment	$\cdots$	0.067 ± 0.003 [41]	5.1 ± 0.4 [41]	0.335 ± 0.075 [42]

TABLE II. Transition form factor $|F(0,0)|$ for $\eta_c(2S)$ at $Q_1^2 = Q_2^2 = 0$.

Potential type	m_c [GeV]	$|F(0,0)|$ [GeV^{-1}]	$\Gamma_{\gamma\gamma}$ [keV]	f_{η_c} [GeV]
Harmonic oscillator	1.4	0.03492	2.454	0.2530
Logarithmic	1.5	0.02403	1.162	0.1970
Powerlike	1.334	0.02775	1.549	0.1851
Cornell	1.84	0.02159	0.938	0.2490
Buchmüller-Tye	1.48	0.02687	1.453	0.2149
Experiment [41]	$\cdots$	0.03266 ± 0.01209	2.147 ± 1.589	

TABLE III. R(0) and $\gamma\gamma$ width for $\eta_c(1S)$ derived in the nonrelativistic limit.

Potential type	R(0) [GeV$^{3/2}$]	$\Gamma_{\gamma\gamma}$ [keV] M = M$_{\eta_c}$	$\Gamma_{\gamma\gamma}$ [keV] M = $2m_c$
Harmonic oscillator	0.6044	5.1848	5.8815
Logarithmic	0.8919	11.290	11.157
Powerlike	0.7620	8.2412	10.297
Cornell	1.2065	20.660	13.568
Buchmüller-Tye	0.8899	11.240	11.409

TABLE IV. R(0) and $\gamma\gamma$ width for $\eta_c(2S)$ derived in the nonrelativistic limit.

Potential type	R(0) [GeV$^{3/2}$]	$\Gamma_{\gamma\gamma}$ [keV] $M = M_{\eta_c}$	$\Gamma_{\gamma\gamma}$ [keV] $M = 2m_c$
Harmonic oscillator	0.7402	5.2284	8.8214
Logarithmic	0.6372	3.8745	5.6946
Powerlike	0.5699	3.0993	5.7594
Cornell	0.9633	8.8550	8.6493
Buchmüller-Tye	0.7185	4.9263	7.4374

$F(0,0)$, together with the resulting decay width into photons $\Gamma_{\gamma\gamma}$, are collected in Table I for the $\eta_c(1S)$ and Table II for the $\eta_c(2S)$, respectively. Rather different results are obtained for different potentials, and they are not always consistent with the one obtained from radiative decay width $\Gamma_{\gamma\gamma}$, rather well known from recent experiments [41]. It is

interesting to compare these—fully relativistic—results to the ones obtained from the wave function at the origin collected in Tables III and IV respectively for $\eta_c(1S)$ and $\eta_c(2S)$. We observe that the relativistic corrections are fairly strong, especially for the Cornell potential.

Also shown in Tables I and II are the values for the so-called decay constant f_{η_c}. In the case of the 1S state, the agreement with a value extracted by the CLEO Collaboration [42] is generally quite good. We wish to point out that the decay constant f_{η_c} is not directly related to the two-photon decay width $\Gamma_{\gamma\gamma}$. Such a relation only exists in the nonrelativistic limit, where both quantities are expressed in terms of the wave function at the origin.

In the upper panel of Fig. 4 we show our results for the normalized $\gamma^*\gamma \to \eta_c$ transition form factor $\tilde{F}(Q^2, 0)$ as a function of photon virtuality (Q^2) for different potential models. Below we will also use the notation $F(Q^2) = F(Q^2, 0) = F(0, Q^2)$, when one of the photons is on shell.
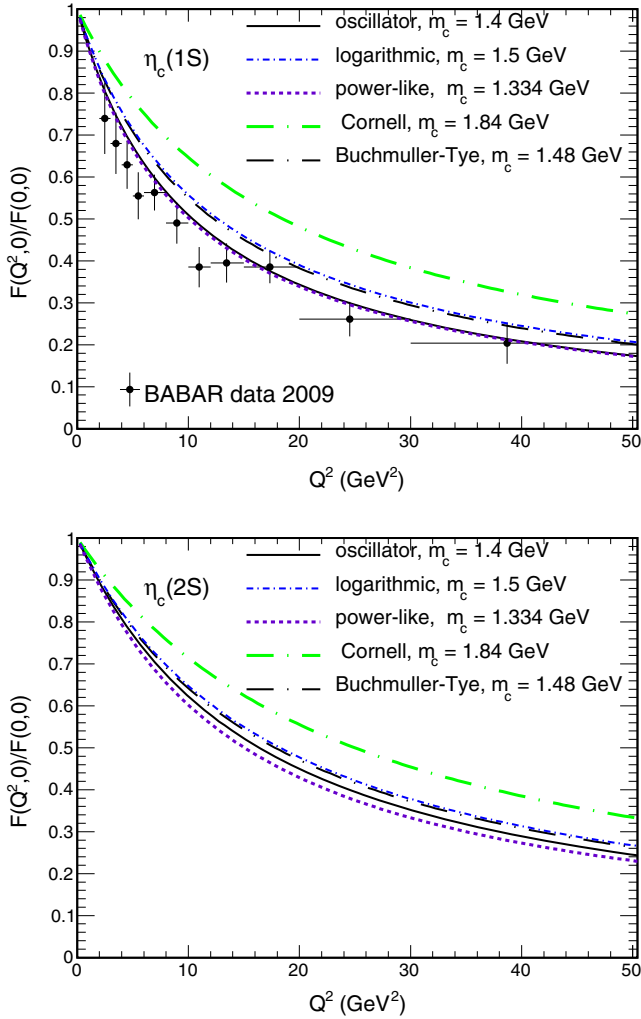

FIG. 4. The dependence of the normalized transition form factor $\tilde{F}(Q^2, 0)$ on spacelike photon virtuality for $\eta_c(1S)$ and $\eta_c(2S)$. For the case of the $\eta_c(1S)$, the BABAR experimental data [20] are shown for comparison.
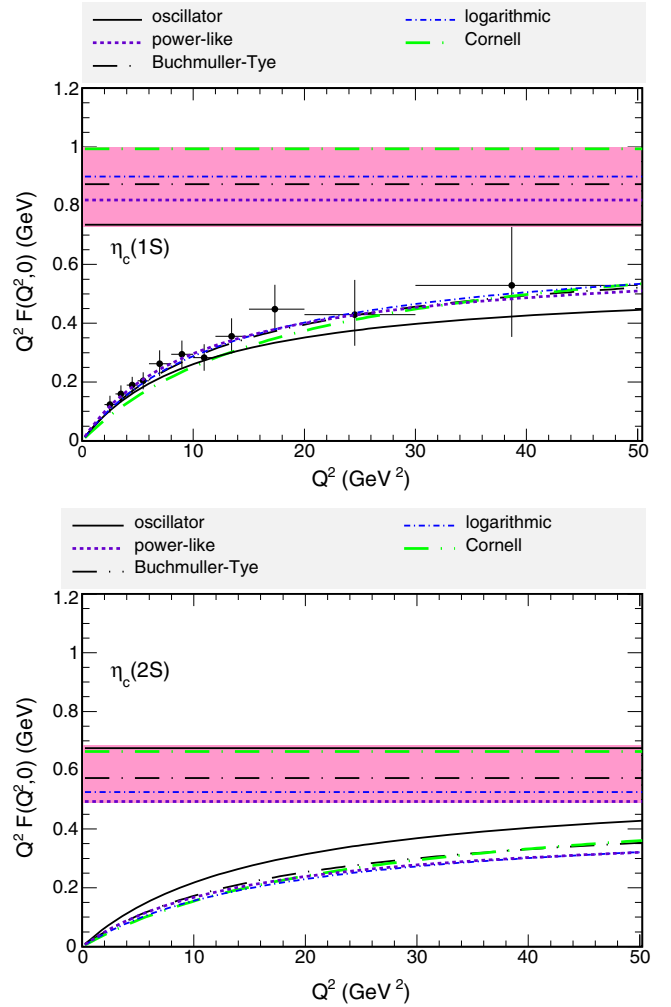
FIG. 5. $Q^2 F(Q^2)$ as a function of photon virtuality for $\eta_c(1S)$ (top) and $\eta_c(2S)$ (bottom) for different potentials used in the present paper.

For reference we also show the *BABAR* experimental data [20]. The oscillator and power-law potentials give the best description of the *BABAR* data. This appears to be related to the lower value of m_c used with these potentials. A modification of the quark mass to $m_c = 1.3$ GeV in the hard matrix element in fact leads to a much better agreement with the *BABAR* data.

The $\gamma^*\gamma$ transition form factor for the $\eta_c(2S)$ is shown in the lower panel of Fig. 4. In this case the $\tilde{F}(Q^2, 0) = \tilde{F}(0, Q^2)$ has a somewhat harder tail as a function of Q^2 than for the $\eta_c(1S)$.

In Fig. 5 we show the rate of approaching of $Q^2 F(Q^2)$ to its asymptotic value predicted by Brodsky and Lepage [38]. For the asymptotic distribution amplitude $\varphi(z, \mu^2) = 6z(1 - z)$, one would obtain $Q^2 F(Q^2) = \frac{8}{3} f_{\eta_c}$. Therefore the horizontal lines $\frac{8}{3} f_{\eta_c}$ are shown for reference [upper panel: $\eta_c(1S)$; lower panel: $\eta_c(2S)$], considering the values for f_{η_c} presented in Tables I and II. We do not observe approaching towards BL asymptotic value for $Q^2 \lesssim 50$ GeV^2. While our results flatten out at large Q^2, their
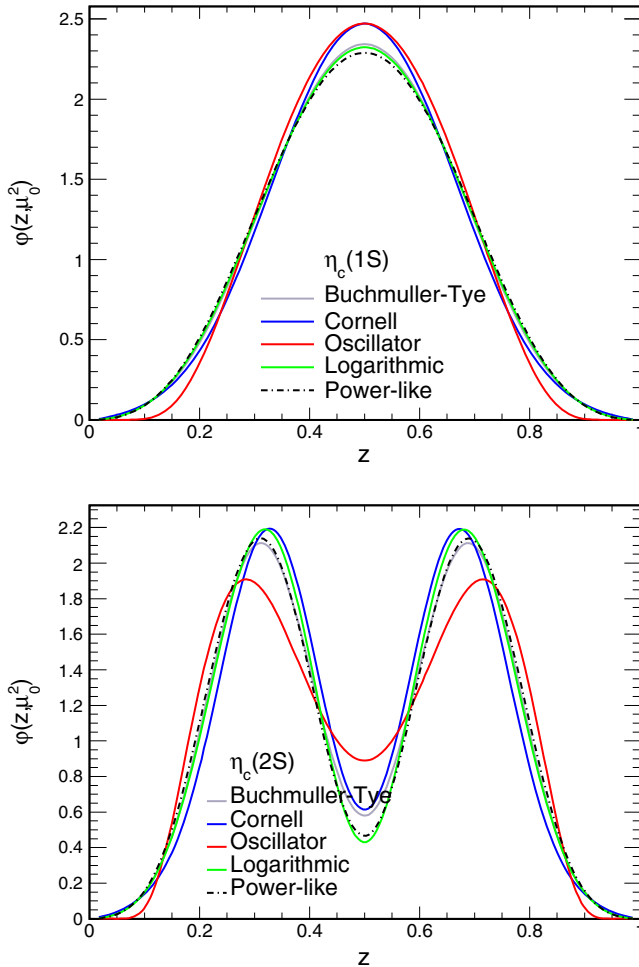
TABLE V. Extracted coefficients $a_n(\mu_0)$, for the Buchmüller-Tye potential.

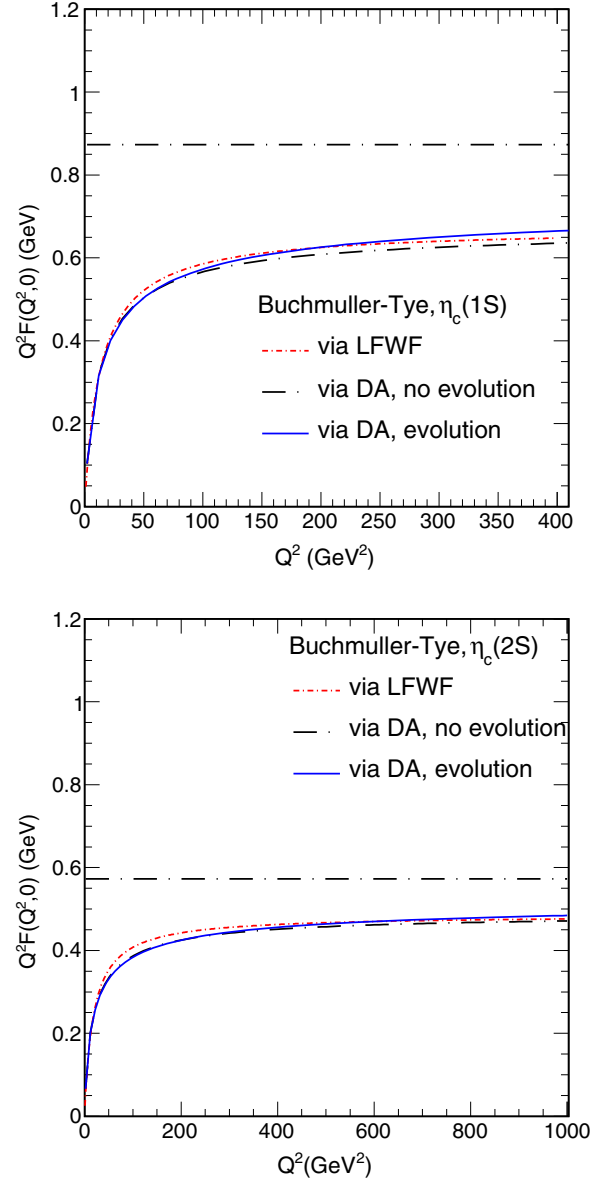| n	$a_n(\mu_0)\eta_c(1S)$	$a_n(\mu_0)\eta_c(2S)$
2	−0.284	−0.0765
4	0.0635	−0.1627
6	−0.008157	0.128
8	−0.000619	−0.049
10	0.000216	0.0088

FIG. 7. $Q^2 F(Q^2)$ for $\eta_c(1S)$ (top) and $\eta_c(2S)$ (bottom) as a function of photon virtuality. The horizontal line is the limit for $Q^2 \to \infty$, calculated for the Buchmüller-Tye potential. The red dashed line (via LFWF) was obtained according to Eq. (2.38). The black dashed-dotted curve (via DA) and the blue solid curve (via DA, evolution) were calculated with Eq. (3.4) respectively with and without evolution of Gegenbauer coefficients a_n.

FIG. 6. Distribution amplitudes for different wave functions for $\eta_c(1S)$ (top) and for $\eta_c(2S)$ (bottom).

asymptotic value is much smaller then the one predicted within the hard scattering formalism.

In order to understand the results for $Q^2 F(Q^2)$ shown above, let us discuss the applicability of a collinear approach, commonly used for light pseudoscalar mesons, for the η_c case. From Eq. (2.49), one has that the collinear formula with the correct asymptotics reads

$$F(Q^2, 0) = F(0, Q^2)$$
$$= e_c^2 f_{\eta_c} \int_0^1 dz \left\{ \frac{z\varphi(z,\mu^2)}{z^2 Q^2 + m_c^2} + \frac{(1-z)\varphi(z,\mu^2)}{(1-z)^2 Q^2 + m_c^2} \right\}.$$
$$(3.4)$$

The evolution with the factorization scale is easily implemented in the formalism of distribution amplitudes. This is routinely done for light pseudoscalar mesons (π^0, η, η'); see e.g., a recent NLO analysis [43]. For $c\bar{c}$ (or $b\bar{b}$) quarkonia the situation is much more complicated and quark mass effects and/or higher twists must be included. In Fig. 6 we show the distribution amplitude at a factorization scale $\mu = 3$ GeV calculated from our wave functions for both $\eta_c(1S)$ and $\eta_c(2S)$. To perform the evolution with the hard scale, the distribution amplitude is expanded with the help of the Gegenbauer $C_n^{3/2}$ polynomials:

$$\varphi(z, \mu^2) = 6z(1-z)(1 + a_2(\mu^2)C_2^{3/2}(2z-1) + \cdots). \quad (3.5)$$

We extract the Gegenbauer coefficients by means of

$$a_n(\mu_0) = \frac{2(2n+3)}{3(n+1)(n+2)} \cdot \int_0^1 dz \varphi(z, \mu_0) C_n^{3/2}(2z - 1). \quad (3.6)$$

They evolve according to

$$a_n(\mu) = a_n(\mu_0) \cdot \left[\frac{\alpha_s(\mu)}{\alpha_s(\mu_0)}\right]^{\gamma_n/\beta_0}, \quad (3.7)$$

with the anomalous dimensions γ_n, which can be found for example in Ref. [38].

For $\eta_c(1S)$, the a_2 coefficient dominates and is typically -0.3 at the initial evolution scale. For the $\eta_c(2S)$ the $n = 4$, 6 coefficients dominate. We show the Gegenbauer coefficients at the scale $\mu_0 = 3$ GeV for both $\eta_c(1S)$ and $\eta_c(2S)$ in Table V.

In Fig. 7 we illustrate the effect of evolution on $Q^2 F(Q^2)$. We compare the result obtained with our original formula, given by Eq. (2.38). In addition, we show results obtained with the collinear formula (3.4) using distribution amplitudes obtained from our light-front wave functions
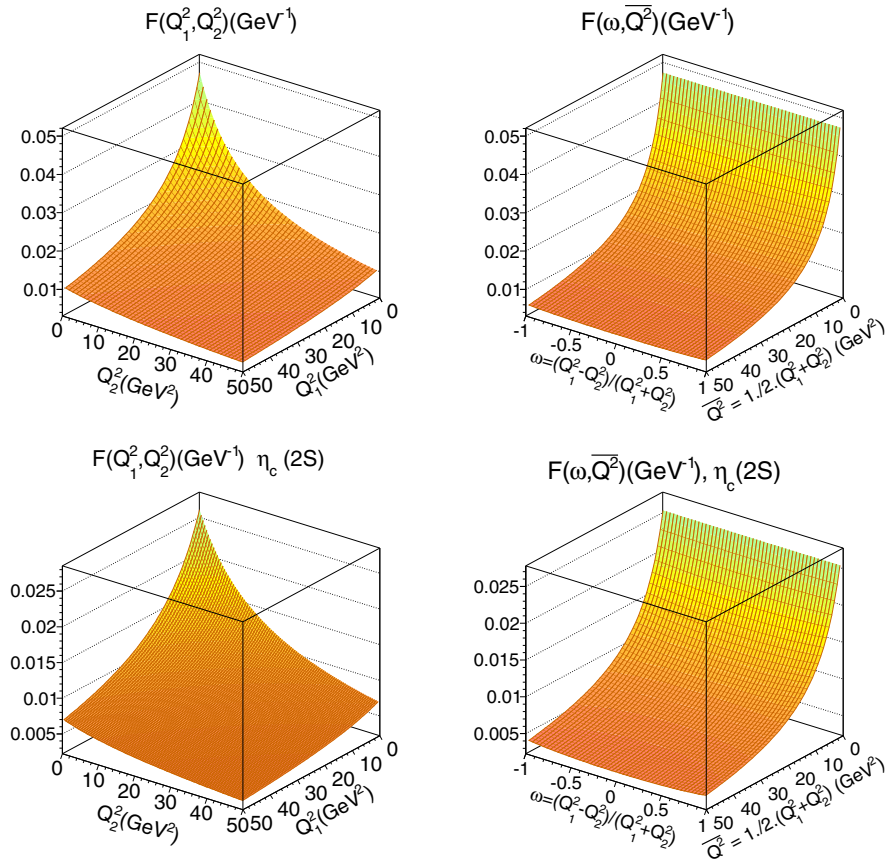

FIG. 8. The $\gamma^*\gamma^* \to \eta_c(1S)$ (top panels) and $\gamma^*\gamma^* \to \eta_c(2S)$ (bottom panels) form factor as a function of (Q_1^2, Q_2^2) and $(\omega, \overline{Q^2})$ for the Buchmüller-Tye potential for illustration; other potentials discussed in the present paper behave similarly.
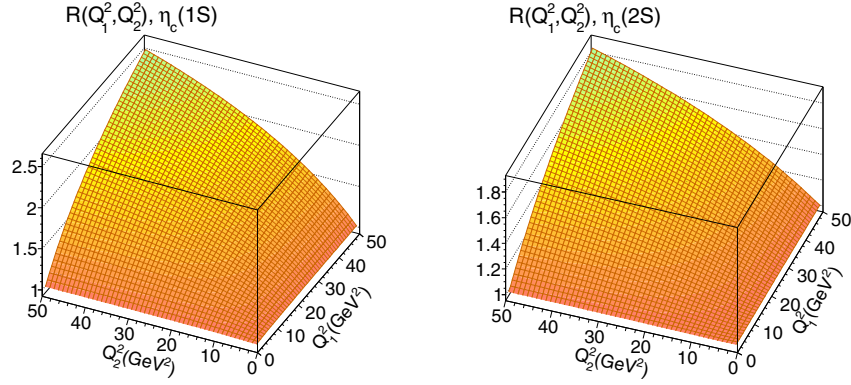
FIG. 9.   Deviations from the factorization breaking (R) as a function of (Q_1^2, Q_2^2) for Buchmüller-Tye potential. Left: $\eta_c(1S)$; right: $\eta_c(2S)$.

(see Fig. 6). There is only some difference at low Q^2. Finally we show also the result obtained within a collinear approach with QCD evolution of distribution amplitudes built in, starting from $\mu_0 = 3$ GeV. The effect of evolution is very weak. The reader is asked to notice a much broader range of Q^2 in the figure compared to that in previous figures. Summarizing, the effect of evolution can be safely neglected for $Q^2 < 100\ GeV^2$, i.e., in the range of our interest, i.e., where $F(Q^2)$ can be measured.

Now we wish to present also two-dimensional distributions for the $\gamma^*\gamma^*$ transition form factor as a function of the photon virtualities Q_1^2 and Q_2^2. As an example in Fig. 8 we again show our results for the Buchmüller-Tye potential. To investigate the scaling properties, we show the transition form factor as a function of the variables

$$\omega = \frac{Q_1^2 - Q_2^2}{Q_1^2 + Q_2^2} \quad \text{and} \quad \bar{Q}^2 = \frac{Q_1^2 + Q_2^2}{2}. \qquad (3.8)$$

One can see that F (and $\tilde{F}$) is almost independent of the asymmetry parameter ω. For comparison, in the $\gamma^*\gamma^* \to \pi^0$ transition discussed in Ref. [44,45], the dependence on ω is somewhat stronger. Note that for the VDM ansatz (3.2) some dependence on ω would be obtained. Future investigation of the slow ω dependence would be in our opinion an interesting task for Belle2.

In Fig. 9 we show deviations from the factorization breaking [see Eq. (3.3)], for the Buchmüller-Tye potential. We observe that $R(0, Q_2^2) = R(Q_1^2, 0) = 1$. The factorization breaking pattern looks very similar for different potentials (not shown explicitly here).

IV. CONCLUSIONS

The description of transition form factors is directly related to our understanding of the structure of bound states in QCD. In the present paper we have studied the transition form factors for $\gamma^*\gamma^* \to \eta_c(1S, 2S)$ for two spacelike virtual photons, which can be accessed experimentally in future

measurements of the cross section for the $e^+e^- \to e^+e^-\eta_c$ process in the double-tag mode. The light-front wave function representation of these observables has been derived and discussed.

We have calculated the transition form factor for different wave functions obtained as a solution of the Schrödinger equation for the $c\bar{c}$ system for different phenomenological $c\bar{c}$ potentials from the literature. The rest-frame momentum space wave functions have been transformed to the light-front representation using the Terentev prescription. First, we have presented the transition form factor for only one off-shell photon as a function of its virtuality and compared to the *BABAR* data for the $\eta_c(1S)$ case. We have also presented the delayed convergence of the form factor to its asymptotic value $\frac{8}{3}f_{\eta_c}$ as predicted by the standard hard scattering formalism. Our results for $Q^2 F(Q^2)$ approach to a lower asymptotic value. The Brodsky-Lepage limit can only be obtained after including QCD evolution of the distribution amplitudes for massless quarks, but appears irrelevant in the accessible kinematic domain. We conclude that it is not necessary to include the QCD evolution for $Q^2 < 100$ GeV^2. This justifies, *a posteriori*, our results obtained within the approach using $c\bar{c}$ wave functions. Furthermore, we have presented two-dimensional distributions in the virtualities of photons of the $\gamma^*\gamma^*\eta_c$ transition form factor for $\eta_c(1S)$ and $\eta_c(2S)$. We have predicted a very slow dependence on the asymmetry parameter ω, which could be verified experimentally at Belle2. We have also defined a measure of factorization breaking and have calculated it for different potentials as a function of (Q_1^2, Q_2^2). The results on the Q_1^2, Q_2^2 dependence are almost model independent.

Finally, it is important to emphasize that the η_c production in hadronic collisions is dominated, at lowest order, by the $g^*g^* \to \eta_c$ subprocess, which is identical (up to global color factors) to the $\gamma^*\gamma^* \to \eta_c$ amplitude derived in this paper. Consequently, our results can also be useful to estimate the η_c production at the LHC, which is currently a theme of intense debate (see e.g., Refs. [46–48]).

ACKNOWLEDGMENTS

[1] V. L. Chernyak and S. I. Eidelman, Prog. Part. Nucl. Phys. **80**, 1 (2015).

[2] A. V. Radyushkin, arXiv:hep-ph/0410276; A. V. Efremov and A. V. Radyushkin, Teor. Mat. Fiz. **42**, 147 (1980) [Theor. Math. Phys. **42**, 97 (1980)]; Phys. Lett. **94B**, 245 (1980).

[3] G. P. Lepage and S. J. Brodsky, Phys. Lett. **87B**, 359 (1979).

[4] V. L. Chernyak and A. R. Zhitnitsky, Phys. Rep. **112**, 173 (1984).

[5] F. Jegerlehner, Springer Tracts Mod. Phys. **274**, 1 (2017).

[6] P. Kroll, Eur. Phys. J. C **71**, 1623 (2011).

[7] N. G. Stefanis, S. V. Mikhailov, and A. V. Pimikov, Few Body Syst. **56**, 295 (2015).

[8] T. Feldmann and P. Kroll, Phys. Lett. B **413**, 410 (1997).

[9] F. g. Cao and T. Huang, Phys. Rev. D **59**, 093004 (1999).

[10] J. J. Dudek and R. G. Edwards, Phys. Rev. Lett. **97**, 172001 (2006).

[11] T. Chen et al. (CLQCD collaboration), Eur. Phys. J. C **76**, 358 (2016).

[12] F. Feng, Y. Jia, and W.-L. Sang, Phys. Rev. Lett. **115**, 222001 (2015).

[13] S. Q. Wang, X. G. Wu, W.-L. Sang, and S. J. Brodsky, Phys. Rev. D **97**, 094034 (2018).

[14] W. Lucha and D. Melikhov, Phys. Rev. D **86**, 016001 (2012).

[15] J. Chen, M. Ding, L. Chang, and Y.-X. Liu, Phys. Rev. D **95**. 016010 (2017).

[16] C. Q. Geng and C. C. Lih, Eur. Phys. J. C **73**, 2505 (2013).

[17] H. Y. Ryu, H. M. Choi, and C. R. Ji, Phys. Rev. D **98**, 034018 (2018).

[18] J. P. Lees et al. (BABAR Collaboration), Phys. Rev. D **98**, 112002 (2018).

[19] J. Cepila, J. Nemchik, M. Krelina, and R. Pasechnik, Eur. Phys. J. C **79**, 495 (2019).

[20] J. P. Lees et al. (BABAR Collaboration), Phys. Rev. D **81**, 052010 (2010).

[21] V. N. Gribov, Y. L. Dokshitzer, and J. Nyiri, Cambridge Monogr. Part. Phys., Nucl. Phys., Cosmol. **27**, 1 (2012).

[22] T. Feldmann, P. Kroll, and B. Stech, Phys. Rev. D **58**, 114006 (1998).

[23] S. D. Glazek and J. Mlynik, Phys. Rev. D **74**, 105015 (2006).

[24] T. Gutsche, V. E. Lyubovitskij, I. Schmidt, and A. Vega, Phys. Rev. D **90**, 096007 (2014).

[25] Y. Li, P. Maris, and J. P. Vary, Phys. Rev. D **96**, 016022 (2017).

[26] M. V. Terentev, Yad. Fiz. **24**, 207 (1976) [Sov. J. Nucl. Phys. **24**, 106 (1976)].

[27] H. J. Melosh, Phys. Rev. D **9**, 1095 (1974).

[28] W. Jaus, Phys. Rev. D **41**, 3394 (1990).

[29] E. Eichten, S. Godfrey, H. Mahlke, and J. L. Rosner, Rev. Mod. Phys. **80**, 1161 (2008).

[30] M. B. Voloshin, Prog. Part. Nucl. Phys. **61**, 455 (2008).

[31] E. Eichten, K. Gottfried, T. Kinoshita, K. D. Lane, and T. M. Yan, Phys. Rev. D **21**, 203 (1980).

[32] E. Eichten, K. Gottfried, T. Kinoshita, K. D. Lane, and T. M. Yan, Phys. Rev. D **17**, 3090 (1978); **21**, 313(E) (1980).

[33] C. Quigg and J. L. Rosner, Phys. Lett. B **71**, 153 (1977).

[34] A. Martin, Phys. Lett. B **93**, 338 (1980).

[35] A. Martin, CERN Reports No. CERN-TH-2876, http://cds.cern.ch/record/133971, 1980.

[36] N. Barik and S. N. Jena, Phys. Lett. B **97**, 265 (1980).

[37] W. Buchmüller and S. H. H. Tye, Phys. Rev. D **24**, 132 (1981).

[38] G. P. Lepage and S. J. Brodsky, Phys. Rev. D **22**, 2157 (1980).

[39] D. Ebert, R. N. Faustov, and V. O. Galkin, Mod. Phys. Lett. A **18**, 601 (2003).

[40] V. A. Novikov, L. B. Okun, M. A. Shifman, A. I. Vainshtein, M. B. Voloshin, and V. I. Zakharov, Phys. Rep. **41**, 1 (1978).

[41] M. Tanabashi et al. (Particle Data Group), Phys. Rev. D **98**, 030001 (2018).

[42] K. W. Edwards et al. (CLEO Collaboration), Phys. Rev. Lett. **86**, 30 (2001).

[43] P. Kroll and K. Passek-Kumericki, Phys. Lett. B **793**, 195 (2019).

[44] S. Ong, Phys. Rev. D **52**, 3111 (1995).

[45] M. Diehl, P. Kroll, and C. Vogt, Eur. Phys. J. C **22**, 439 (2001).

[46] M. Butenschoen, Z. G. He, and B. A. Kniehl, Phys. Rev. Lett. **114**, 092004 (2015).

[47] H. Han, Y. Q. Ma, C. Meng, H. S. Shao, and K. T. Chao, Phys. Rev. Lett. **114**, 092005 (2015).

[48] H. F. Zhang, Z. Sun, W. L. Sang, and R. Li, Phys. Rev. Lett. **114**, 092006 (2015).